Journal of Fluids Engineering

Technical Briefs

Study of Drag Forces on a Designed Surface in Bubbly Water Lubrication Using Electrolysis

Haosheng Chen
State Key Laboratory of Tribology,
Tsinghua University,
Beijing, 100084 China
e-mail: chenhs@mail.tsinghua.edu.cn

Jiang Li
Department of Mechanology,
University of Science and Technology,
Beijing, 100083 China

Darong Chen
State Key Laboratory of Tribology,
Tsinghua University,
Beijing, 100084 China

To study the drag reduction effect of a bubbly fluid, a pin-disk experiment is performed on the Universal Micro Tribotester system. Bubbles are generated by water electrolysis in holes that are specially designed on the disk surface. Experiment result shows that the drag force experiences a dynamic process, both drag reduction and drag increment effects appear in the process depending on the bubble behavior. This process is numerically simulated using computational fluid dynamics (CFD), and the explanations for the drag variation are given based on the analysis of drag forces on each wall of the disk surface. The drag reduction occurs when the bubble fills the hole, as the viscous drag on the air-liquid surface is small, and the pressure drag is reduced as the side wall of the hole is covered by the bubble. The drag increment is thought to be caused by the increment of the fluid viscosity when the bubble leaves the hole and flows in the fluid.
[DOI: 10.1115/1.2354531]

Keywords: bubble, drag reduction, lubrication, surface roughness

1 Introduction

Water and water-based lubricants, such as emulsions, are widely used in metalworking lubrication and journal bearing lubrication [1–5]. The good lubricating properties of water-based lubricants have been studied for many years [1]. In most of the studies, the lubricant is seen as single phase or is treated as a discontinuous oil phase dispersed in a continuous water phase. But bubbles cannot be avoided in journal bearing lubrication as a previous study result [2] has pointed out. It is known that the effective viscosity of the bubbly mixture may decrease [3], but at times, the bubbly mixture show a negative effect on lubrication. Results in journal bearing lubrication provided by An et al. [2] and Nikolajsen [6] indicate that the viscosity of the bubbly oil increases and the friction force also increases. Studies on drag reduction give the same conclusion: the bubbles do not cause the drag reduction in laminar flow as they do in a turbulent boundary layer [7,8]; lubricants are often in laminar flow in journal bearing lubrication.

However, some conditions of the studies need to be noted here. First, the surface is considered to be smooth in such studies and the surface roughness is not included. Nevertheless, the surface roughness, such as the grooves and holes on the surface, has been shown to have important effects in journal bearing lubrication [9,10]. Second, since the bubbles are injected into the water in most of the drag reduction experiments [11,12], the condition that the bubbles are in the holes or grooves is not considered.

The goal of this ongoing study is to explore whether drag reduction can occur in laminar flow under the effect of designed surface roughness and controlled bubbles. A pin-disk friction experiment is designed using water lubricants; the Universal Micro Tribotester (UMT) system is used to measure the friction force at the pin-disk interface. Water electrolysis is used to generate bubbles in the lubrication, which is also adopted in the pioneering experiment done by McCormich and Bhattacharyya [13]. A board with holes on the surface is designed as the disk, and the bubbles are generated in the holes. In the experiment, both the bubbles' generation speed and the bubble size can be controlled, so the drag force in laminar flow with different bubble characteristics is investigated. Four models are established and the bubbly lubrication process is numerically simulated. The explanation for the drag variation is also given based on the analysis of the forces on the different walls. According to the instrument used in this experiment, the results are restricted in the oscillating machinery, and the laminar flow condition is satisfied as the fluid film thickness is usually considered very small.

2 Experimental

2.1 Bubble Generation. Here, water electrolysis is adopted to generate bubbles, and the bubble generation speed is controlled by the supply voltage; a special board is designed to control the size and position of the bubbles. The specially designed board is a kind of two-layer printed circuit board. Its structure and shape are shown in Fig. 1, where the unit of the dimension is millimeter.

The board is made of PTFE (polytetrafluoroethylene); the completed board is shown in Fig. 1(*c*), which is 37 mm wide and 46 mm long. The structure of the board with holes is shown as the cross section A-A in Fig. 1(*a*). The top surface of the board is covered by a thin gold layer, whose thickness is <10 μm, and the

Contributed by the Fluids Engineering Division of ASME for publication in the JOURNAL OF FLUIDS ENGINEERING. Manuscript received November 15, 2005; final manuscript received May 8, 2006. Assoc. Editor: Theodore Heindel.

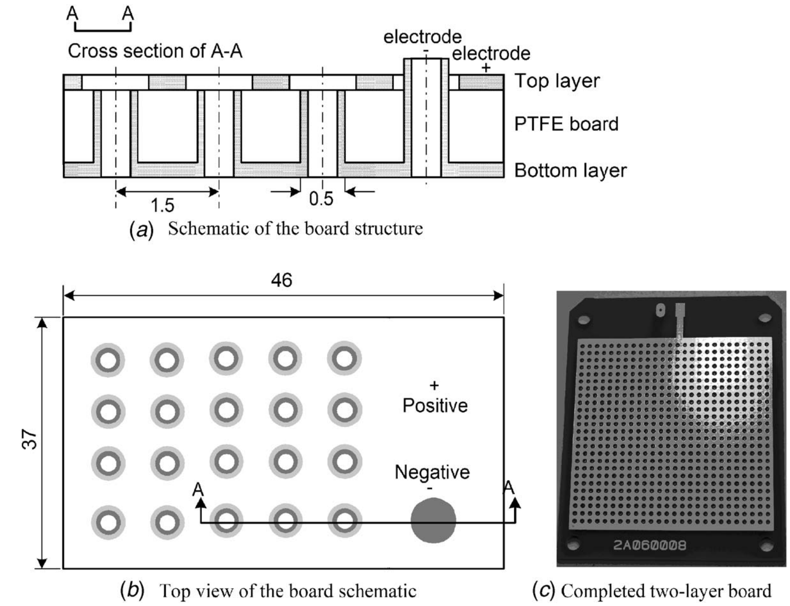

Fig. 1 Structure of the two-layer printed circuit board

layer is connected to the positive pole of the power supply; thus, the whole top layer acts as the positive electrode. In the same way, the whole bottom layer is connected to the negative pole of the power supply.

There is an array of holes through the board. Each hole's diameter is 500 μm, and the interval between two holes is 1.5 mm. The inner surface of each hole is also covered by a thin gold layer, and the layers inside the holes are connected with each other through the bottom layer. Because there is an insulation layer outside the bottom layer, all the inner surfaces of the holes act as the negative electrodes. In the experiment, the board will be dipped into the electrolyte, and a supply voltage will be added on the two electrodes to begin the water electrolysis. The water is electrolyzed and the bubble is generated in the hole. The position and the size of the bubble are controlled by the position and the diameter of the designed hole, whereas the speed of generation is controlled by the supply voltage.

2.2 Experimental Schematic. The schematic of the pin-disk friction force test setup is shown in Fig. 2. The pin is installed on a UMT system; the friction force and normal force on the pin surface are tested by the two-dimensional sensor of the system. The pin's position can be adjusted in the system, and the load of the pin on the disk can be controlled from 0 to 500 g. The printed circuit board is used as the disk; it is installed in the electrolyzing cell which is fixed on the carriage of the UMT system. As the carriage performs a reciprocating movement, whose speed is controlled by the UMT system, the top layer of the circuit board is considered as a moving surface, while the pin can be considered as the stationary surface in the pin-disk interface lubrication.

The electrolyzing cell is filled with the water lubricant. The water lubricant is a saturated salt (NaCl) solution. 0.25% HEC (hydroxyethylcellulose) is added into the solution to increase the solution's viscosity, in case that the friction force variation is too

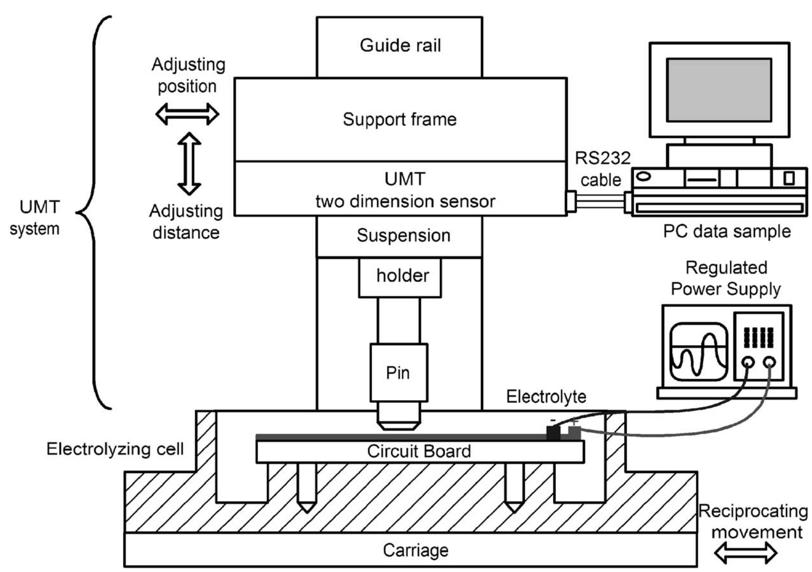

Fig. 2 Experimental system schematics

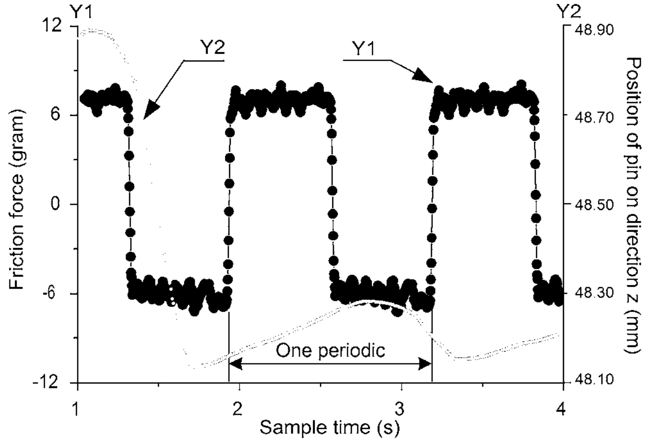

(a) Friction forces at 1.0V voltage under 50 gram load

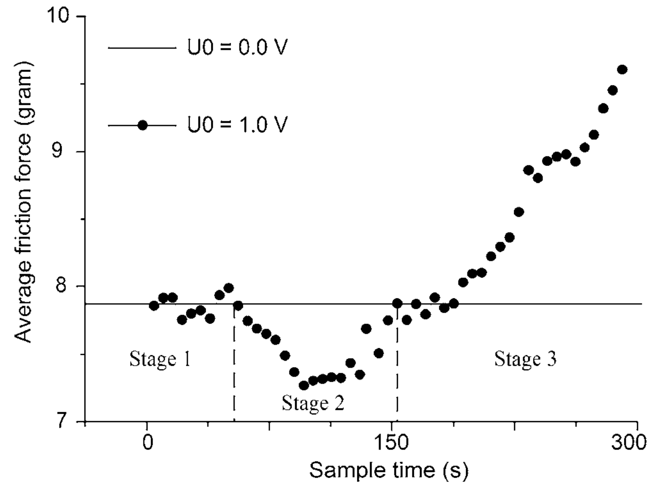

(b) Average friction forces at 1.0V voltage under 50 gram load in 300 seconds

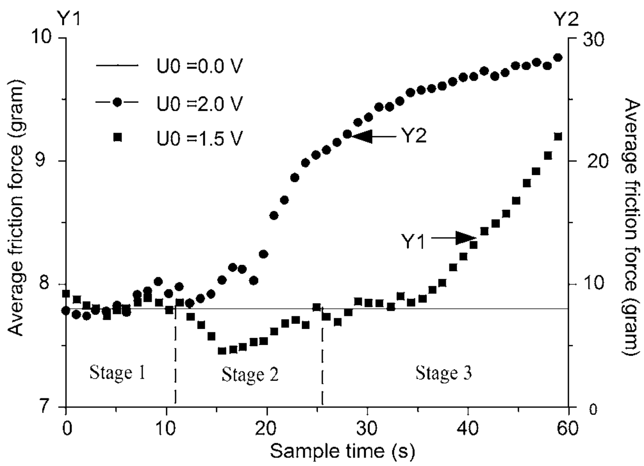

(c) Average friction forces under 50 gram load in 60 seconds

Fig. 3 Drag forces on the designed surface under difference supply voltages: (*a*) Friction forces at 1.0 V voltage under 50 g load, (*b*) average friction forces at 1.0 V voltage under 50 g load in 300 s, and (*c*) average friction forces under 50 g load in 60 s

small to be tested by the sensor. Two electrodes are connected to the power supply through two enamel wires. Once the voltage is supplied to the board, the water electrolysis begins in the cell. The gas in the bubbles are considered to be hydrogen because the bubbles are observed firstly in the holes with the negative electrode on the wall, then the bubbles are rising from the holes to the water surface and form a bubble array according to the positions of the holes. During this process, the bubbles' effect on the friction force in pin-disk interface lubrication is investigated.

2.3 Experimental Results. The air originally remaining in the holes is driven out using an ultrasonic cleaner before the experiment. Then the load of the pin is adjusted to 50 g, and the supply voltage is adjusted to 1.0 V. The carriage of the UMT system performs a reciprocating movement at the speed of 1 cm/s, as soon as the voltage is supplied on the electrodes of the disk. The testing lasts 300 s, and a trace of the friction forces on the pin surface at the beginning of the test is shown in Fig. 3(*a*). In the figure, the time for completing a whole reciprocating movement is called one periodic. Because the friction force is always opposite to the pin's moving direction, half of the data have positive values while the others have negative values in one period.

It should be noted here that the lubricating regime is thought to be in hydrodynamic condition because of two reasons. One is the friction coefficient. According to the experiment data, the friction coefficient calculated is lower than 0.2; the other is the position variation of the pin on direction z (perpendicular to the disk surface). At the beginning of the test, the pin contacts the disk surface under the load of 50 g. When the reciprocating movement is performed, the pin is automatically adjusted according to the pressure on the pin surface. The data of the position shown in Fig. 3(*a*) suggest that the pressure on the pin surface increases and the pin moves upward, which indicates that hydrodynamic lubricating occurs in the pin-disk interface.

The whole process of the friction force variation during the testing is shown in Fig. 3(*b*). In the figure, each point on the curve represents the average value of the positive friction forces in a half period; U0 represents the supply voltage for the water electrolysis. It is found from the result that the force variation is not monotonic, and it can be divided into three stages shown in Fig. 3(*b*). In stage 1, the friction forces on the pin surface almost keep constant, and no bubble is observed on the board surface. It is considered that the reaction time of the water electrolysis is not long enough for the bubbles to have an effect on the friction force. In the next few minutes of stage 2, the friction force on the surface decreases, and the forces are lower than the drag force at the beginning of the electrolysis. It indicates that the drag reduction

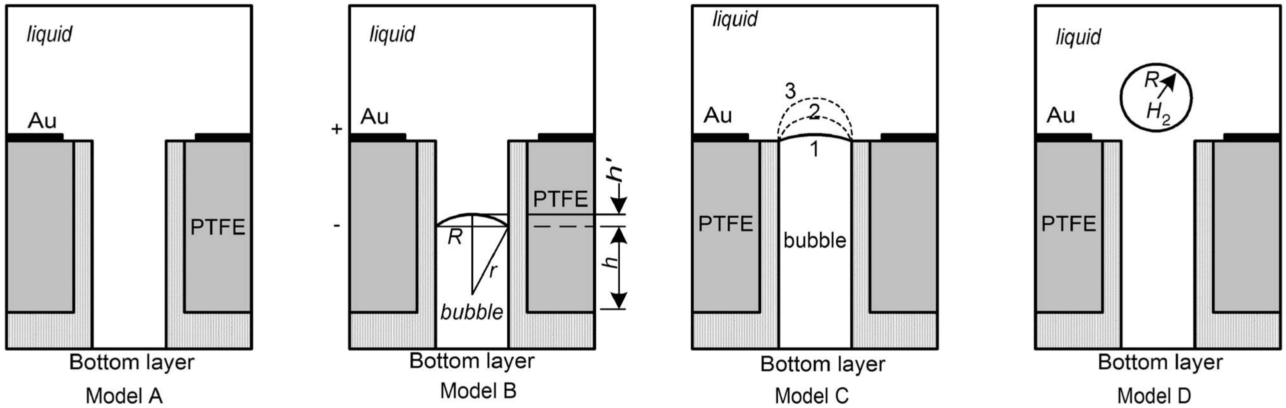

Fig. 4 Models for the bubbly lubrication in different stages

effect occurs under the experimental condition; thus, stage 2 may be called drag reduction stage. In this stage, a few bubbles appear on the board surface. In the last minutes of stage 3, the friction force increases rapidly as the water electrolysis continues, and it exceeds the drag force at the beginning of the electrolysis. It is predicted that the drag force increment cannot be avoided in the lubrication at last. In this stage, a lot of bubbles are observed to leave the holes and aggregate in the solution.

The expected drag reduction effect that occurred in the experiment lasts about 100 s under the voltage of 1.0 V. However, the continuous time of the effect depends on the electrolysis supply voltage. The continuous time of the drag force reduction effect under different voltages is shown in Fig. 3(*c*). The continuous time is shortened obviously when the supply voltage increases to 1.5 V. Moreover, when the supply voltage is high enough, for example, reaching 2.0 V in this experiment, the continuous time decreases, or even disappears as shown in Fig. 3(*c*). In such condition, the water electrolysis becomes strenuous, and the bubbles grow so fast that they leave the holes as soon as they are generated.

From the results, it is determined that the drag reduction effect can be realized even in laminar flow under the effect of bubbles, and the bubble behavior at different stages plays an important role in the drag force variation. Numerical analysis is provided as follows to give the explanations for the bubbly lubrication process.

The experimental error and uncertainty are discussed here. Take the data shown in Fig. 3(*b*) for example, each point in Fig. 3(*b*) represents the average value of the positive friction forces in a half period shown in Fig. 3(*a*). The bias limit is about ±0.364 at 95% confidence, and the uncertainty in the experiment result is ±0.217 using the sequential perturbation method [14]. The experiment has been performed three times and the uncertainty is ±0.254. Since the UMT is a kind standard tester machine and it is calibrated before the experiment, it is believed that the system error has been compensated already.

3 Numerical Analysis on Experimental Results

3.1 Models and Method. It is considered that the status of the bubble in the hole changes at different stages of the experiment. According to the dynamic process of drag force variation in the experiment, four models are established for calculating the drag forces at different stages. The schematics of the four models A, B, C, and D are shown in Fig. 4.

For model A, the water electrolysis begins or just lasts for a short time; no bubble is generated in the hole and the hole is filled with water. For model B, a bubble appears in the hole as the water electrolysis continues, and an air-liquid surface is formed. Because the contact angle of the water on the gold surface is <90 deg, a concave meniscus is formed. Two parameters are used to describe the shape of the bubble, one is called the bubble height h and the other is the curvature radius r of the air-liquid surface. The bubble height is increasing as the water electrolysis continues, while the curvature radius remains almost constant when the bubble is in the hole. In such condition, the hole is small enough to be seen as a capillary and the surface is considered as a part of a sphere. The simplified Laplace equation (1) [15] is used to calculated the curvature radius r.

$$\Delta P = \frac{2\sigma}{r} \tag{1}$$

where ΔP is the pressure difference in and outside of the bubble, σ is the surface tension force, g is the gravity acceleration. With the two parameters, the shape of the air-liquid surface is determined. As the electrolysis continues, the bubble height will reaches the hole depth, then model C is used. In this model, the bubble's height stays constant and equal to the hole's depth, but the curvature radius continues to decrease until it reaches the hole's radius. This process is shown as the dashed lines in model C; it is like the traditional maximum bubble pressure testing process. The curvature radius of the bubble will continues to increase after it reaches the hole's radius. However, such a bubble is unstable under shearing force and such status is not considered in this paper. As the electrolysis continues, the bubble will eventually leave the hole and go into the water solution. Thus, the bubbly lubricant is formed, and model D is adopted to calculate the drag force on the surface. For model D, the viscosity of the fluid is changed because there are a lot of bubbles in the solution. Here, the viscosity is calculated as the modified viscosity equation (2) provided by Sugden [15]. Where η_b is the bubbly lubricant's viscosity, η_0 is the water's viscosity, and β is the bubble content.

$$\eta_{\mathrm{b}} = \eta_0(1 + 0.015\beta) \tag{2}$$

It should be noted that the four models take effect periodically and sequentially during the electrolysis. For example, when the bubble goes into water in model D, the water fills the hole and it is electrolyzed again. Then, a few bubbles are formed and the bubble will experience the next three models sequentially again. As the result, more and more bubbles aggregate in the lubrication.

With these models, the drag force on the surface in different stages can be calculated. However, the calculation is based on some conditions and assumptions stated as follows:

1. The fluid is in the laminar flow condition. This condition can be satisfied because the moving speed is adjusted to be small enough.
2. The real 3D experiment is represented by the 2D models shown in Fig. 4 in the calculation. This substitution affects the model precision, but it makes the calculation easy to be realized with current computers.
3. Although some polymer additives are added into the salt

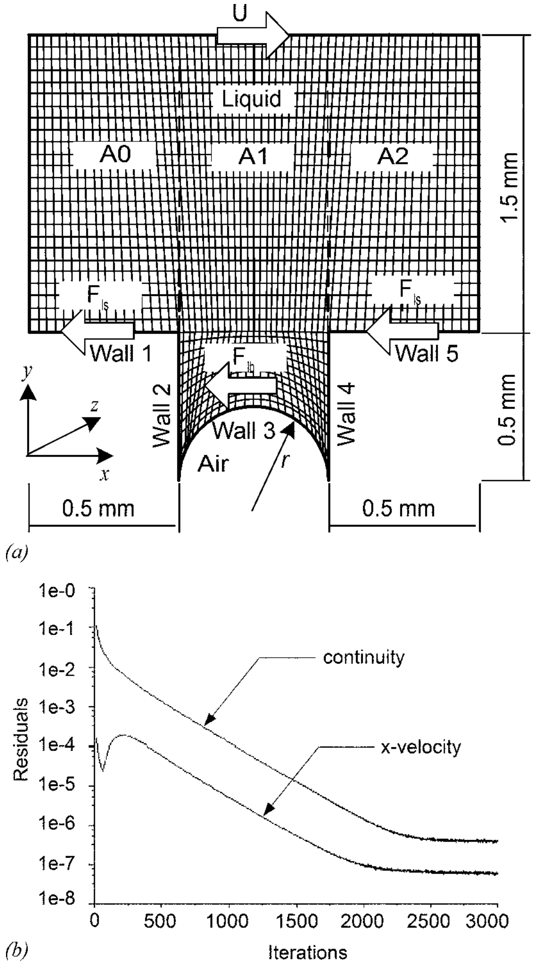

Fig. 5 Preprocessing and residuals for numerical simulation: (*a*) mesh and walls of model B and (*b*) residuals of the numerical results

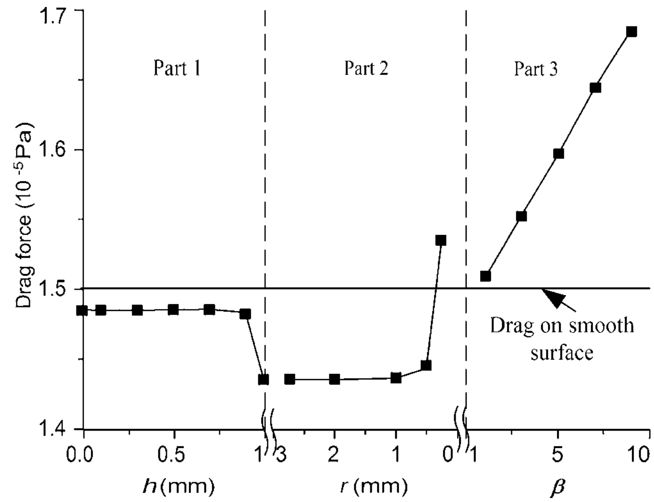

Fig. 6 Numerical simulation on drag force variation process

water to increase the viscosity, the solution is still treated to have a constant viscosity because the shear rate is kept constant.

4. It is considered that the hole is a kind of capillary, and the air-liquid surface is a part of spherical surface. Eq. (1) is established on the basis of this condition.
5. It is assumed that the curvature of the air-liquid surface keeps unchanged as the bubble height grows. When the bubble height is equal to hole depth, the curvature reduces until it reaches the hole's radius.
6. It is assumed that the radius of the bubble is equal to the hole's radius after it leaves the hole and stays in the solution. It is a simplification method to make the calculation easy.

Usually, the Reynolds equation is used in hydrodynamic lubrication calculations, but the models provided here have steep-walled roughness, and the depth of the hole is in the same order of the fluid thickness, so the traditional Reynolds equation is not applicable [16,17]. In this paper, the CFD software FLUENT is used to calculate the drag force on the surface. As a common method, FLUENT uses a control-volume-based technique to convert the governing equations to algebraic equations that can be solved numerically, which is called finite volume method. The continuity equation and momentum equation are adopted in the calculation, which are applicable for any continuous medium. The forces and pressures on different walls under the effect of bubbles are shown in Fig. 5(*a*). The bottom surface has been divided into five walls. The viscous force F_{ls} exists on solid-liquid surfaces (wall 1 and wall 5), while the viscous force F_{lb} exists on air-liquid surface (wall 3); pressure drag appears on the side wall 2 and 4. The total drag force on the surface consists of forces on different walls of the bottom surface.

The boundary conditions are defined as follows: the upper surface is a moving wall with the speed of 1 cm/s; the bottom surface consists of five stationary walls; the left side is a pressure inlet and the right side is a pressure outlet. However, some special conditions need to be added for different models. For models B and C, the air-liquid surfaces are treated as a "slip" wall, which means that there is a tangential velocity component in terms of the translational motion of the wall boundary. Nevertheless, the shear stress on the surface is considered to be zero. For model D, the viscosity of the fluid is calculated according to Eq. (2). Here, the lubricant is considered to perform a stable laminar flow, and the laminar model is adopted here.

Here, the residual definitions are used for judging convergence. This criterion requires that the residuals decrease to 10^{-6} for the continuity equation and velocity equation. The variations of the residuals are shown in Fig. 5(*b*). The residuals both reach the convergence criteria and almost keep constant after 2500 iteration steps, which indicate that the numerical process is converged. To show the pressure and fluid flow near the air-liquid surface more obviously, the mesh number is increased from the center to the wall and the grow factor is 1.1, which is also shown in Fig. 5(*a*). The grid size is about $20\times 20\ \mu\text{m}^2$, which is small enough in laminar flow compared to the size of hole marked in Fig. 5(*a*).

3.2 Lubrication Process Simulation. The calculated drag force on the pin surface during the whole process is shown in Fig. 6. It is found that the one simulated process is very like the real drag force variation process in the experiment, but what should be noted here is that the simulated process consists of three parts using different models, each part is numbered according to stages of the drag force variation in experiment that has been described in Fig. 3.

In Part 1, the drag force variation under different bubble heights has been shown, it corresponds with the experimental data in stage 1. When the bubble height is zero, model A is used to calculate the drag force, otherwise, model B is used in this part. It is found in Part 1 that the bubble's size does not show obvious effect on the drag force as the bubble is growing in the hole until the height is near the hole depth. At the end of Part 1, the bubble's height is very close to the hole depth, and model C is adopted. According to Eq. (1), the curvature radius is 2.73 mm. As the electrolysis continues, the curvature radius reduces until it reaches the hole radius 0.25 mm. The drag forces under different curva-

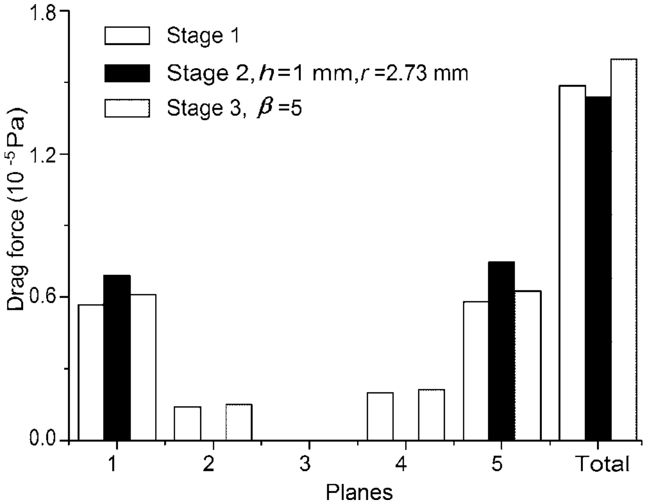

Fig. 7 Drag forces on different walls of the surface

ture radius are shown in Part 2. Only in this part, the drag reduction effect can be obviously observed. However, the drag reduction does not last the whole part. The drag force is increasing as the bubble curvature radius reduces, and it gets a correspondingly high value when it is equal to the hole's radius. This result corresponds with the experiment data in stage 2, and it indicates that only model C can produce the drag reduction effect in laminar flow. Model D is adopted in part 3, and the drag force increases as the bubble content β increases in the bubbly lubrication. The drag force seems to have a linear relationship with the bubble content in Fig. 6. In the calculation, the bubble content changes from 1 to 9; but in fact, the bubble content changes in a more complex manner, because some bubbles are generated in the hole while other bubbles are disappearing in the water. Thus, such a result exists only under a simplified condition.

It should be noted here that, although the process is periodic, the drag reduction effect only can be observed in the first period, because the water will be filled with bubbles after stage 3 of the first period, and the rapidly increased drag force will overcome the drag reduction effect that occurs in stages 1 and 2, which has been shown by the experiment results.

3.3 Analysis of Forces on Walls. Forces on different walls are analyzed to investigate the variation of drag force during the different stages. As shown in Fig. 5, walls 1, 3, and 5 are parallel to the $x-z$ wall, and are called parallel walls; wall 2 and wall 4 are perpendicular to the $x-z$ wall and are called perpendicular walls. On perpendicular walls, there are pressure drags, whereas on parallel walls, there are viscous drags. Here, the force on each wall is obtained using the finite volume method as discussed above, and the forces on each wall in different stages are compared in Fig. 7. Because the drag forces in model A and B are almost the same, model A is omitted and model B is used in stage 1. Models C and D with determined parameters are used in stage 2 and 3, respectively.

It can be seen that the drag force on bottom plane (plane 3) of the hole in all the three stages are very small because the flow velocity is rapidly decreased in the hole (i.e., the shear force is decreased, which leads to the decrement of viscous drag on the bottom plane). Although the loss of the forces on the bottom wall of the hole is compensated by the pressure drag on the perpendicular walls, the loss of the viscous force is higher than the acquired pressure drag. Compared to a smooth surface, a little drag reduction is acquired in stage 1 under this surface roughness.

In stage 2, there is small or even no pressure drag on perpendicular planes, because the perpendicular planes are almost covered by the bubble. Although the viscous drags on the parallel planes (walls 1 and 5) in stage 2 are higher than those in stage 1 and 3, the increment of the viscous drag cannot compensate for the loss of pressure drag, so there is a lower drag force in stage 2 than in stage 1. Compared to a smooth surface, the surface with holes seems to have less contact area with fluid because the shear stress on wall 3 is omitted, so there is less viscous drag on the surface. Also, there is no pressure drag to compensate for the loss of viscous drag. Thus the drag reduction appears. However, the arc height of the air-liquid surface increases when the curvature radius reduces, which causes the increment of the pressure drag on the surface. As a result, the drag force on the bottom surface increases, which corresponds with the drag increment part in stage 2 of the experiment.

In stage 3, forces on every wall are higher than those in stage 1, because the viscosity of the bubbly lubricant is higher than that of lubricant without bubbles. According to Eq. (2), the viscosity of the lubricant increases as the bubble content increases, which leads to the increment of the drag force. This numerical result also corresponds with the experimental data in stage 3.

From what has been discussed above, we can conclude that in stage 1, surface roughness is the reason of a little drag reduction effect; in stage 2, the bubble's shape is the dominant factor that causes an obvious drag reduction; in stage 3, the increment of the fluid's viscosity causes the drag increment.

4 Discussion

It is found that the drag reduction effect appears when the liquid-solid surface is partly substituted by the air-liquid surface. However, there is the question of whether the air-liquid surface has enough load capacity to bear the pressure generated in the hydrodynamic lubrication. In Sec. 3.1, the curvature radius of the air-liquid surface is calculated under the condition that there is only the stationary fluid pressure on the surface. In fact, the pressure on the surface will be higher when the hydrodynamic pressure is formed. An iteration process of the pressure and the surface shape are needed to calculate the curvature radius considering the hydrodynamic pressure. It is a really complex process, and it is not realized in this paper. However, we still have a choice to use the bubbly lubrication technology, even when the air-liquid surface cannot support the hydrodynamic pressure because we can design a surface with smaller holes. The pressure on one air-liquid surface will be afforded by more surfaces with smaller radius. It is an attractive study to investigate the relationship between the lubrication and bubble size; but, it is also another problem that is not discussed here.

5 Conclusions

In this experiment, bubbles are generated by water electrolysis, and the bubble's size and position are controlled by the specially designed surface. The bubbly lubrication is seen as a periodic and dynamic process, as the bubble changes status from staying in the hole to staying in the fluid film. During the process, a drag reduction effect appears even in laminar flow. After the drag reduction stage, the drag force on the surface increases rapidly. Based on the calculated forces on the walls, some conclusions are drawn as follows:

1. The bubbles have little effect on the drag force at the beginning of the water electrolysis, and the surface roughness causes a little drag reduction.
2. An obvious drag reduction can be acquired when the bubble height is close to the hole's depth. The reason is that the viscous drag on the air-liquid surface is omitted due to the slip wall effect, while the pressure drag on the side wall is also avoided because the side wall is almost totally covered by the bubble. However, the drag force will increase as the air-liquid surface grows, because the pressure drag appears and it increases as the surface arc height increases.
3. When the bubble leaves the hole and goes into the lubricat-

ing film, the bubbly lubricant is formed. Because the viscosity of the bubbly lubricant is higher than liquid, the drag force on the surface increases. The increment of the drag force in this stage will cover the drag reduction effect in the experiment as the electrolysis continues.

Acknowledgment

The authors would like to thank Han Zhonglin (Tsinghua University) for his contributions toward this work. This work is supported by the Research Fund for the Doctoral Program of Higher Education (Grant No. 20030003026), NSFC Project (No. 50505020), and NSFC Project (No. 50475018).

Nomenclature

g = gravity acceleration
h = height of the bubble
r = bubble's curvature radius
U = velocity of the moving wall
$U0$ = supply voltage
R = radius of the hole on circuit board

Greek Letters

σ = surface tension force
η_b = bubbly lubricant's viscosity
η_0 = water viscosity
β = bubble content in the fluid
ΔP = pressure difference in and outside of the bubble

References

[1] Boure, P., Mazuyer, D., and Georges, J. M., 2002, "Formation of Boundary Lubricating Layers With Water-Based Lubricant in a Concentrated Elastohydrodynamic Contact," ASME J. Tribol., **124**, pp. 91–102.
[2] An, Q., Zhou, Y. S., and Quan, Y. X., 1997, "Study on the Viscosity Properties of Bubbly Oil and the Static Characteristics of Journal Bearing Lubricated With Bubbly Oil," Wear, **213**, pp. 159–161.
[3] Hayward, A. T. J., 1962, "The Viscosity of Bubbly Oil," J. Inst. Pet., **48**, pp. 156–164.
[4] Kimura, Y., and Okada, K., 1989, "Lubricating Properties of Oil In Water Emulsions," Tribol. Trans., **32**, pp. 524–532.
[5] Schmid, S. R., and Wilson, R. D., 1996, "Lubrication Mechanisms for Oil-In-Water Emulsions," Lubr. Eng., **52**, pp. 168–175.
[6] Nikolajsen, J. L., 1999, "The Effect of Aerated Oil on the Load Capacity of a Plain Journal Bearing," Tribol. Trans., **42**, pp. 58–62.
[7] Madavan, N. K., Deutsch, S., and Merkle, C. L., 1985, "Numerical Investigation Into the Mechanisms of Micro Bubbles Drag Reduction," ASME J. Fluids Eng., **107**, pp. 370–377.
[8] Deutsch, S., Money, M., and Fontaine, A. A., 2003, "Microbubble Drag Reduction in Rough Walled Turbulent Boundary Layers With Comparison Against Polymer Drag Reduction," *Proceedings of 4th ASME/JSME Joint Fluids Engineering Conference*, ASME, New York, Vol. 2, Part A, pp. 665–673.
[9] Wang, L. L., and Cheng, I. W., 1997, "An Average Reynolds Equation for Non-Newtonian Fluid With Application to the Lubrication of the Magnetic Head-Disk Interface," Tribol. Trans., **40**(1), pp. 111–119.
[10] Chiang, H. L., and Hsu, C. H., 2004, "Lubrication Performance of Finite Journal Bearings Considering Effects of Couple Stresses and Surface Roughness," Tribol. Int., **37**, pp. 297–307.
[11] Kato, H., Miyanaga, M., and Haramoto, Y., 1994, "Friction Drag Reduction by Injecting Bubbly Water Into Turbulent Boundary Layer," *Cavitation and Gas-Liquid Flow in Fluid Machinery and Devices*, Fluids Engineering Division, ASME, New York, Vol. 190, pp. 185–194.
[12] Yoon, H. S., Kim, W. J., and Kim, H. T., 2003, "Experimental Study on the Drag Reduction by Injection of Microbubble and Polymer Solution in a Water Tunnel for Water-borne Vehicles," *Proceedings of 4th ASME/JSME Joint Fluids Engineering Conference*, ASME, New York, Vol. 2, Part A, pp. 705–712.
[13] McCormick, M. E., and Bhattacharyya, R., 1973, "Drag Reduction of a Submersible Hull by Electrolysis," Nav. Eng. J., **85**, pp. 11–16.
[14] Figliola, R. S., 2000, *Theory and Design for Mechanical Measurements*, Wiley, New York.
[15] Sugden, S., 1922, "Determination of Surface Tension from the Maximum Pressure in Bubbles," J. Chem. Soc., **121**, pp. 858–859.
[16] Elrod, H. G., 1979, "A General Theory for Laminar Lubrication With Reynolds Roughness," ASME J. Tribol., **101**, pp. 8–14.
[17] Almqvist, T., and Larsson, R., 2004, "Some Remarks on the Validity of Reynolds Equation in the Modeling of Lubricant Film Flows on the Surface Roughness Scale," ASME J. Tribol., **126**, pp. 703–709.